JACS
JOURNAL OF THE AMERICAN CHEMICAL SOCIETY

Article

pubs.acs.org/JACS

Analyte-Driven Switching of DNA Charge Transport: *De Novo* Creation of Electronic Sensors for an Early Lung Cancer Biomarker

Jason M. Thomas,[†,‡] Banani Chakraborty,[†] Dipankar Sen,*[,†,‡] and Hua-Zhong Yu*[,†]

[†]Department of Chemistry and [‡]Department of Molecular Biology and Biochemistry, Simon Fraser University, Burnaby, British Columbia V5A 1S6, Canada

Supporting Information

ABSTRACT: A general approach is described for the *de novo* design and construction of aptamer-based electrochemical biosensors, for potentially any analyte of interest (ranging from small ligands to biological macromolecules). As a demonstration of the approach, we report the rapid development of a made-to-order electronic sensor for a newly reported early biomarker for lung cancer (CTAP III/NAP2). The steps include the *in vitro* selection and characterization of DNA aptamer sequences, design and biochemical testing of wholly DNA sensor constructs, and translation to a functional electrode-bound sensor format. The working principle of this distinct class of electronic biosensors is the enhancement of DNA-mediated charge transport in response to analyte binding. We first verify such analyte-responsive charge transport switching in solution, using biochemical methods; successful sensor variants were then immobilized on gold electrodes. We show that using these sensor-modified electrodes, CTAP III/NAP2 can be detected with both high specificity and sensitivity (K_d ~1 nM) through a direct electrochemical reading. To investigate the underlying basis of analyte binding-induced conductivity switching, we carried out Förster Resonance Energy Transfer (FRET) experiments. The FRET data establish that analyte binding-induced conductivity switching in these sensors results from very subtle structural/conformational changes, rather than large scale, global folding events. The implications of this finding are discussed with respect to possible charge transport switching mechanisms in electrode-bound sensors. Overall, the approach we describe here represents a unique design principle for aptamer-based electrochemical sensors; its application should enable rapid, on-demand access to a class of portable biosensors that offer robust, inexpensive, and operationally simplified alternatives to conventional antibody-based immunoassays.

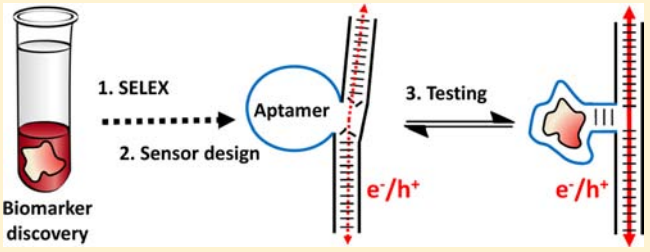

INTRODUCTION

DNA aptamers have emerged as effective and robust recognition elements for use in molecular biosensors for analytes ranging from small molecules to biomacromolecules.[1] Even whole cells have been detected and/or captured using aptamers.[2] Analytical readouts from aptamer-based biosensors most commonly derive from global-scale conformational changes or "structure switching" in the aptamer domain by analyte binding.[3] For example, optical readouts based on FRET (Förster Resonance Energy Transfer) or fluorescence quenching have proven successful, where structure switching upon analyte binding causes a change in distance between two chromophores attached to the aptamer.[3] In the case of aptamer-based electrochemical biosensors, numerous designs have been reported involving electrode-bound aptamers and either diffusible or covalently tethered redox labels.[4] Most commonly in these systems, changes in electrochemical signal derive from alteration of the distance between the electrode surface and a redox label appended to the aptamer; as a result, the rate of direct electron transfer between the electrode and redox label is responsive to analyte binding. Changes in electrode to redox label distance can arise due to (1) analyte binding-induced folding or global conformational change in single stranded, electrode-bound aptamers,[5] (2) displacement of oligonucleotides from double stranded, electrode-bound aptamer complexes prompted by analyte binding,[6] or (3) sandwich binding of an analyte between an unlabeled, electrode-bound aptamer and a secondary, redox-labeled aptamer in solution.[7] In the past few years, we have been exploring a unique biosensor design principle that represents a distinct alternative to the above paradigms.[8−10] The function of the class of biosensors we describe, termed "deoxyribosensors", is designed to depend on the integrity of duplex DNA-mediated charge transport between an electrode and a redox label (*vide infra*),[11] rather than on distance-dependent, direct charge transfer.[5,6]

Moving beyond model sensors that are based on well-characterized aptamers,[5,6,8−10] in this paper we report the *de novo* creation of made-to-order deoxyribosensors for novel lung cancer biomarkers, blood-borne proteins for which no aptamer sequences have been reported to date. Lung cancer claims more than 1.2 million lives per year and is the leading cause of cancer mortality worldwide.[12] Early detection can dramatically increase

Received: June 6, 2012
Published: July 26, 2012

   dx.doi.org/10.1021/ja305458u | *J. Am. Chem. Soc.* 2012, 134, 13823−13833

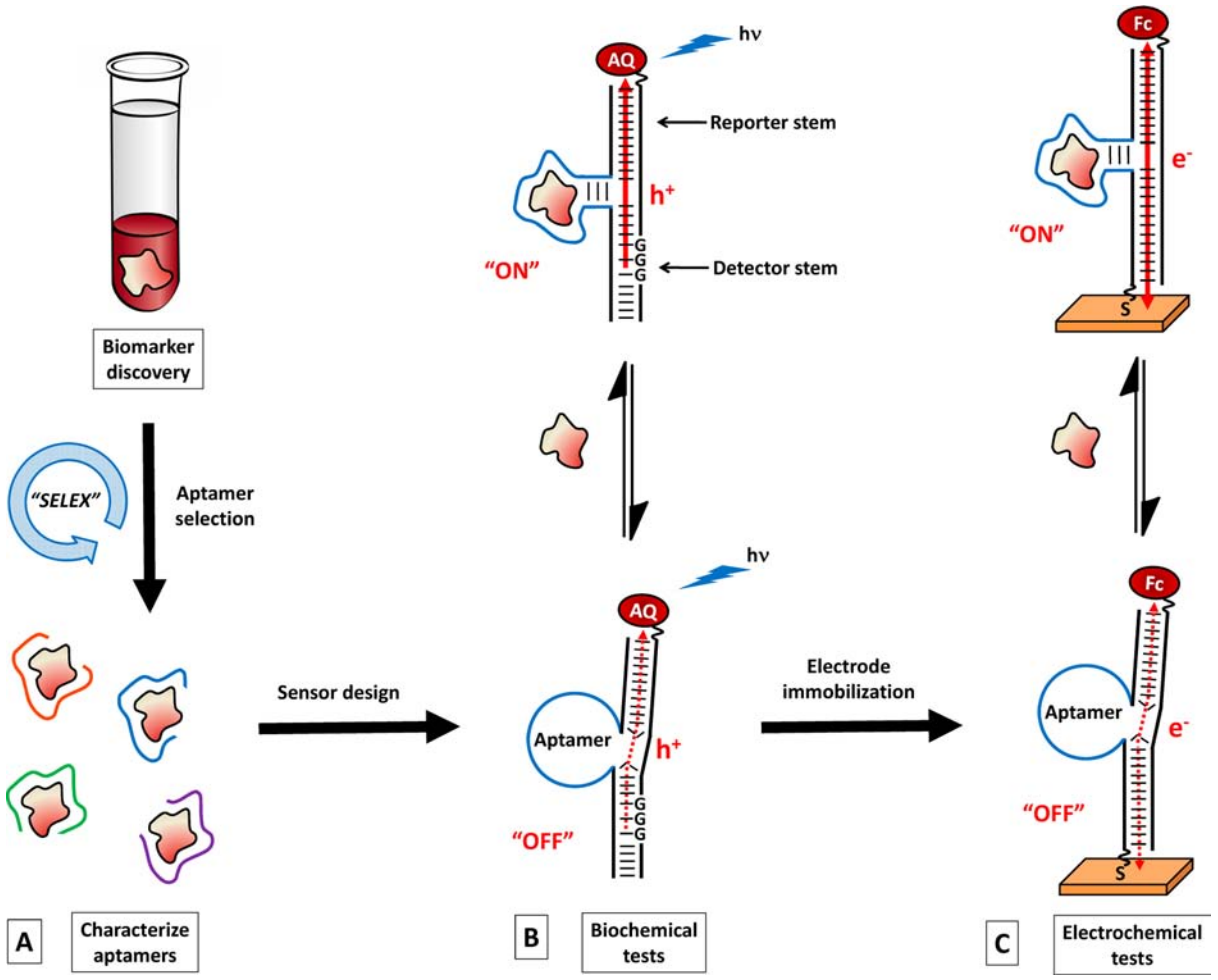

Figure 1. Illustration of the *de novo* creation of deoxyribosensors for newly discovered biomarkers. Aptamers for the analyte of interest are generated using SELEX. Suitable aptamers are then incorporated into the sensor constructs, which are initially tested biochemically, in solution. The analyte binding-induced through-DNA charge transport is detected by monitoring guanine oxidation in the detector stem resulting from charge migration (in the form of an electron hole, h^+) to a photoexcited anthraquinone (**AQ**) tethered to the reporter stem. Sensors that are functional in solution are then tested electrochemically, where the sensor mediates reversible charge transport between the electrode to which it is bound and a covalently tethered redox label (ferrocene, **Fc**).

survival rates, however, current diagnostic tests (e.g., CT scans or bronchoscopy) capable of detecting submillimeter sized tumors are not practical for large-scale screening of the general population.[13] Recent clinical research has shown that elevation of the combined serum concentrations of connective tissue activating peptide-III (CTAPIII) and neutrophil activating peptide-2 (NAP2) serves as powerful indicators for lung cancer, even in its earliest stages.[13−15] CTAPIII and NAP2 are two chemokine proteins derived from the same preprotein (they differ only by a 15 amino acid extension at the N-terminus of CTAPIII).[16] To address the need for a cost-effective screening test to evaluate lung cancer risk, we have undertaken the *de novo* development of an electronic sensor capable of sensitive quantification of CTAPIII+NAP2 levels in serum samples. We envision that such sensors will form the basis of a simple, inexpensive, point-of-care test that will enable population-wide screening for high lung cancer risk.

As illustrated in Figure 1, the design and construction of functional deoxyribosensors for a newly discovered biomarker analyte requires the following milestones: (A) *in vitro* selection of high-affinity and -specificity aptamers that bind the desired target, and characterization of such aptamers to determine their suitability for incorporation into a deoxyribosensor; (B) biochemical testing of various three-way junction designs to maximize the change in through-DNA charge transport efficiency in response to analyte binding; (C) optimization of the electrochemical performance of promising deoxyribosensor candidates bound to gold electrodes as self-assembled monolayers (SAMs). In the "coupled ligand deoxyribosensor" (CLD) design detailed herein, a three-way junction is formed by inserting an aptamer domain between two conductive, double helical stems (the reporter and detector stems). Ideally, analyte binding-generated folding/conformational changes in the aptamer domain induce alignment and interhelical stacking of the reporter and detector stems. This interhelical stacking constitutes "electrical contact" and facilitates electron−hole transport through the three-way junction between the reporter and detector stems. On the basis of this charge transport switching principle, even subtle changes in aptamer conformation could potentially be transduced into an enhanced electrochemical signal. In contrast, more global scale conformational changes or secondary structure rearrangements are required in systems that are designed to function based on modulation of direct electron transfer between the electrode

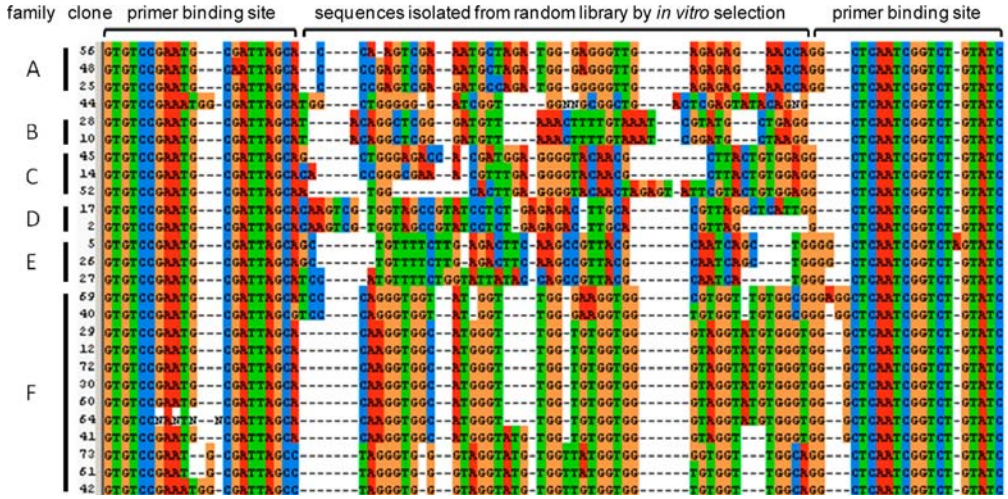

Figure 2. DNA sequences isolated following 15 rounds of *in vitro* selection for anti-CTAP III aptamers.

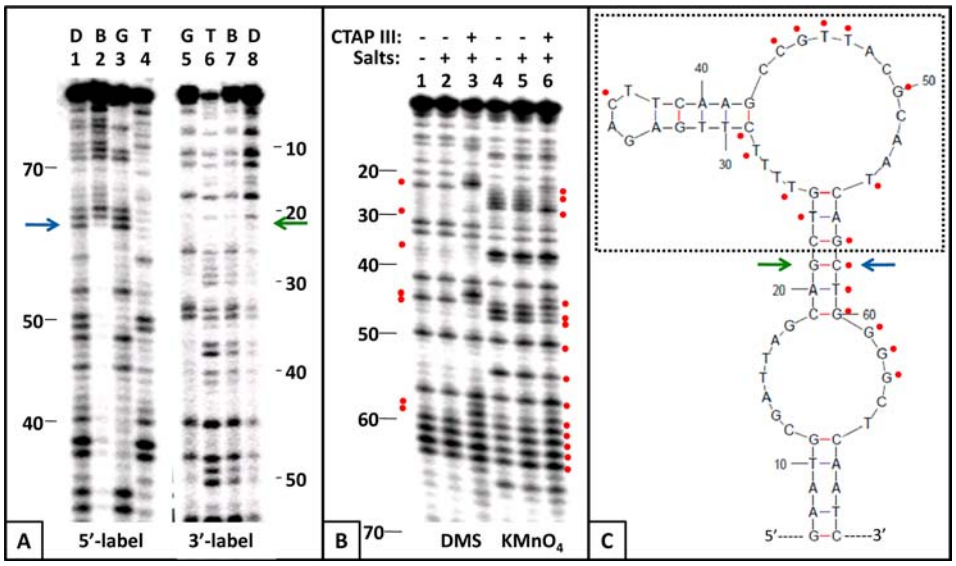

Figure 3. (A) Aptamer boundary-mapping experiments to determine the minimally required aptamer sequence for clone 27. Lanes D, sequence fragments not bound to CTAPIII resin; lanes B, sequence fragments bound to CTAPIII resin; lanes G, G-specific sequencing ladder; lanes T, T-specific sequencing ladder. Lanes 1−4 are 5′-^{32}P labeled samples and lanes 5−8 are 3′-^{32}P labeled samples. The blue and green arrows denote the first required nucleotide at the 3′- and 5′-ends, respectively, of the "core" aptamer domain. (B) Dimethylsulfate (DMS, lanes 1−3) and $KMnO_4$ (lanes 4−6) reactivity protection assays for clone 26. Significant changes in reactivity upon CTAPIII binding are marked by red dots. (C) Secondary structure predicted by mFold for clone 26. The aptamer domain is marked to correspond to the data in Figure 3A, and the sequence incorporated into the CLD lies within the dashed box. Changes in nucleotide reactivity to DMS or $KMnO_4$ are marked to summarize data in Figure 3B. Extraneous sequences from the primer binding sites at the 5′- and 3′-termini have been omitted for clarity.

and the redox label tethered to the DNA.[5,6] To address the question of whether such a mechanism contributes to the enhanced electrochemical signal in our electrode-bound sensors, we have used FRET experiments to probe for global-scale sensor conformational changes that might accompany analyte binding. The fact that we observe negligible structural change upon analyte binding argues against a direct, distance-dependent charge transfer switching mechanism. Instead, these findings support a through-DNA conductivity switching mechanism for the electrode-bound sensors that is consistent with the unequivocally observation of such a mechanism in solution. Evidently, this common charge transport switching mechanism depends on very subtle conformational changes that affect helical alignment and base stacking at the three-way junction.

RESULTS AND DISCUSSION

Anti-CTAPIII/NAP2 Aptamer Selection and Characterization. We used an affinity chromatography-based SELEX approach,[17] where aptamer sequences were partitioned based on binding to CTAP III that had been conjugated to an agarose solid support. Starting with a library of ~10^{14} single-stranded DNA incorporating a 40-nucleotide random region, we isolated six distinct CTAPIII/NAP2-binding aptamer families (Families A-F, Figure 2) after 15 rounds of selection. The final DNA pool is clearly dominated by heavily G-rich aptamers (e.g., Family F), which likely form G-quadruplex structures (see Supporting Information). Family F aptamers indeed showed high affinity for CTAP III/NAP2, although it remained to be investigated if they possessed suitable properties for sensor design. A detailed

dx.doi.org/10.1021/ja305458u | J. Am. Chem. Soc. 2012, 134, 13823−13833

account of CTAPIII/NAP2 aptamer selection is given in the Supporting Information.

In evaluating the suitability of specific aptamers for incorporation into CLDs, we first sought to remove extraneous sequences from the cloned aptamer sequences. To ensure that oligonucleotides used to construct deoxyribosensors remain of reasonable length (<70 nt), the aptamer domain should not exceed 40 nt. We performed boundary mapping experiments (Figure 3A and Supporting Information) to define the minimally required sequence of various selected aptamers. 5′- or 3′-^{32}P-labeled aptamer sequences were randomly fragmented, and the boundaries of functional aptamer domains were defined by those fragments that retained affinity for CTAP III. On the basis of the boundary data in Figure 3A for clone 27, Family E aptamers were minimized to 36 nt. Electrophoretic mobility shift assays (Figure 4) confirmed that the minimized Family E aptamers retained high affinity for CTAP III, with K_d = 14 ± 3 nM.

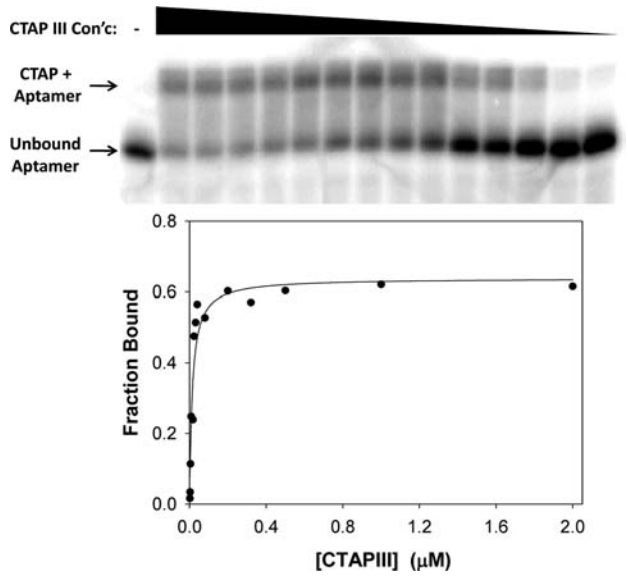

Figure 4. Measurement of the CTAPIII binding affinity of aptamer 27−1 by native gel electrophoretic mobility shift analysis. Aptamer 27-1 is a truncated version of the clone 27 aptamer (see Supporting Information). The K_d value was determined to be 14 ± 3 nM.

In fact, aptamer minimization dramatically improved the extent of aptamer binding to the target relative to the full 80 nt sequence (see Supporting Information); evidently, the presence of the extraneous sequences caused significant misfolding of the full length Family E aptamer sequences. According to secondary structure prediction (Figure 3C), the 3′- and 5′-termini of the minimized Family E aptamers form a short helical stem, which would be an ideal point of attachment to complete the three-way junction of a CLD. It is desirable that aptamer termini should be arranged spatially in proximity to one another, so as to facilitate grafting onto the CLD construct without detriment to aptamer folding. In this regard, G-quadruplex-based aptamers (e.g., Family F) may cause complications due to the unpredictability of quadruplex topology and thus of the spatial orientation of termini. This caveat notwithstanding, in cases where topology is well-defined, such as for the well characterized antiparallel G-quadruplex of the thrombin aptamer, CLD design has been successful.[10]

Aptamers suitable for use in CLDs should also exhibit detectable conformational change upon analyte binding. To investigate this, we carried out reactivity protection assays in which the extent of reaction of individual aptamer nucleotides with DNA-modifying reagents varies with conformational changes resulting from CTAPIII binding. Figure 3B shows the results for clone 26 (Family E), where reactivity changes for numerous nucleotides are readily apparent, consistent with discernible conformational change upon CTAPIII binding. Especially promising for CLD design was the observation of reactivity changes in several nucleotides in the helical stem through which the aptamer would be attached between the reporter and detector stems of the CLD (Figure 3C). In light of all of the above characterization, Family E aptamers were judged to be the best candidates for incorporation into initial designs of CLDs.

Sensor Construction and Biochemical Characterization. With high affinity CTAP III aptamers defined, the next challenge was to find specific three-way junction sequences that would give rise to functional CLDs. Efficient charge transport through a three-way junction in response to analyte binding requires facilitated stacking between the reporter and detector stems in the analyte-bound state. Although general guidelines have been reported for predicting coaxial stacking in bulged three-way junctions,[18] these are not expected to strictly apply to CLDs owing to deviations from ideal duplex structure at the point of attachment of the aptamer domain. Therefore, we tested six junction sequences, which represent a comprehensive range of structural space possible for a three-way junction, in search of the most pronounced difference in biochemical charge transport in response to CTAP III binding (Figure 5). Junction variants incorporated, variously, two nucleotide bulges at the 3′- and 5′-termini of the aptamer domain (CLD constructs **S1** and **S2**, Figure 5B), and a completely base-paired junction (CLD **S3**, Figure 5B). CLD **S3** showed the most pronounced concentration-dependent increase in charge transport in the presence of CTAP III, as visualized by strand cleavage at oxidized guanine residues in the detector stem (lanes 4, 5, and 6, Figure 5B). Therefore, CLD **S3** was carried forward for testing in an electrochemical sensor format. It should be noted that this three-way junction structure (CLD **S3**) is not the same as those adapted for the deoxyribosensors for adenosine[8] or thrombin,[10] indicating that each sensor design is unique as a result of its particular aptamer folding and conformational change.

Sensor Immobilization and Electrochemical Validation. To convert CLD **S3** into an electrochemical sensor, the detector stem was altered to remove the easily oxidized guanine triplet present in the biochemical sensor format. The 5′-terminus of the aptamer strand was modified with a hexanethiol linker to enable robust attachment to a gold electrode surface. Finally, the anthraquinone (AQ) moiety tethered to the 5′-terminus of the complementary strand was replaced with ferrocene, which exhibits reversible one-electron redox behavior suitable for electrochemical measurements.[19] Square wave voltammetry was used to test the gold chip-immobilized CLD **S3**, as well as a negative control construct that consisted of a fully complementary duplex with the same sequence found in the charge conduction pathway of the CLD. Square wave voltammograms showed substantial increase in the peak current for CLD **S3** upon addition of 100 nM CTAPIII in binding buffer (Figure 6A), whereas the peak current for duplex DNA was relatively unchanged (Figure 6B). We also examined the

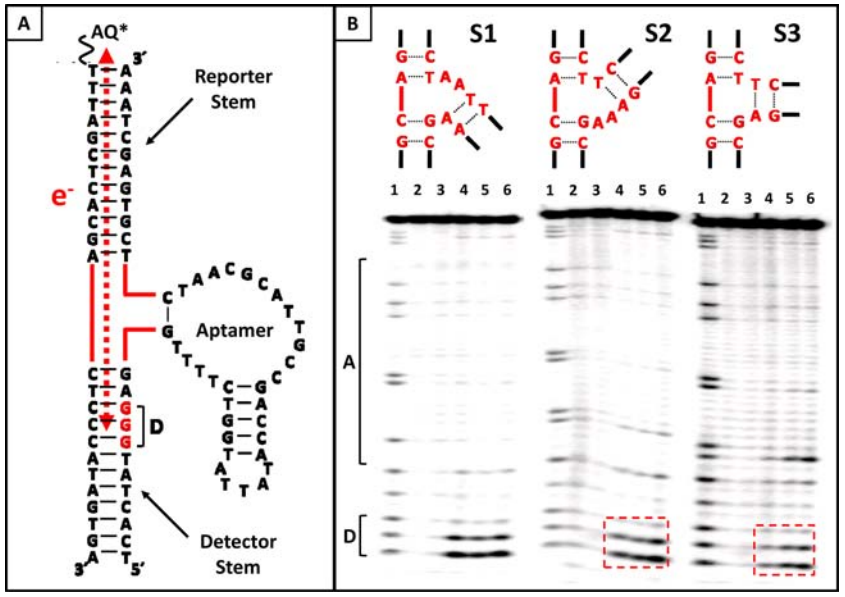

Figure 5. (A) Design of CLD constructs that incorporate the clone 27 aptamer. Irreversible charge transfer occurs between the detector stem guanine triplet (red, denoted "D") and photoexcited anthraquinone (AQ*). Various three-way junction sequences (solid red lines) were tested. (B) Biochemical charge transport assays for three-way junction variants **S1**, **S2**, and **S3**. Charge transfer to photoexcited anthraquinone (AQ) is revealed by piperidine-induced cleavage at oxidized reporter stem guanines (denoted by D and red boxes). The aptamer domain is denoted by A. Lane 1, G-specific sequencing ladder; lane 2, negative control (UV irradiation with no appended AQ); lane 3, negative control (no UV irradiation); lane 4, UV irradiation without CTAPIII; lane 5, UV irradiation with 20 nM CTAPIII; lane 6, UV irradiation with 200 nM CTAPIII. The binding buffer contained 50 mM Tris-HCl (pH 8.0), 25 mM KCl, and 1 mM $MgCl_2$.

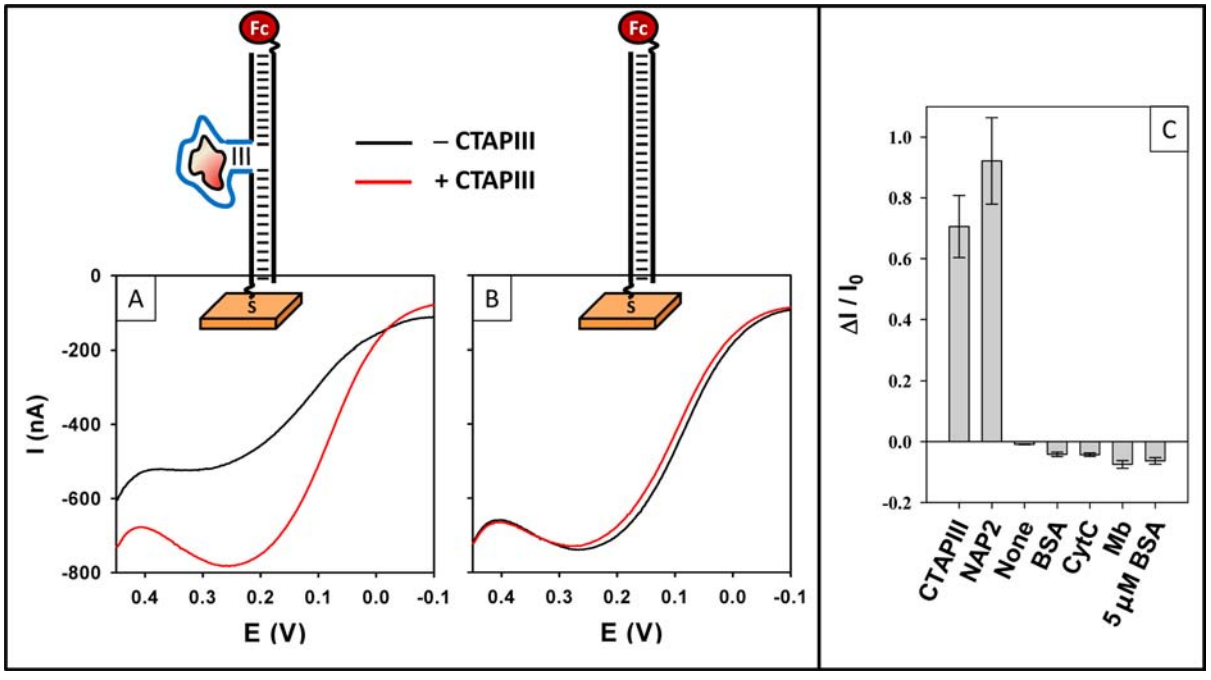

Figure 6. Representative square-wave voltammograms for (A) CLD **S3** and (B) a fully complementary duplex DNA, each bound to a gold electrode via C6-thiol linker. The black and red voltammograms were collected with 0 nM and 100 nM CTAPIII, respectively. (C) Relative peak current change for CLD **S3** in the presence of various proteins (100 nM unless otherwise indicated). BSA = bovine serum albumin; CytC = cytochrome C; Mb = myoglobin.

specificity of the CLD **S3** by measuring its response to the presence of control proteins. As shown in Figure 6C, a small, but discernible *decrease* in peak current was observed for CLD **S3** in the presence of three negative control proteins, such as cytochrome C (Cyt C), myoglobin (Mb), and bovine serum albumin (BSA).

Consistent with earlier observations in the detection of thrombin using a different CLD system,[10] sensitivity increased by an order of magnitude on conversion from the biochemical to the electrochemical sensor format (upon shortening of the conductive stems and immobilization on gold electrode surface). Binding isotherms generated from electrochemical

dx.doi.org/10.1021/ja305458u | J. Am. Chem. Soc. 2012, 134, 13823–13833

results for CLD **S3** (Figure 7A) yielded similar apparent dissociation constants (K_d) for CTAP III and NAP2, of 1.2 ± 0.1 and 2.4 ± 0.2 nM, respectively (with NAP2 binding producing a significantly higher peak current at saturation). The median CTAPIII + NAP2 concentrations in the sera of healthy and lung cancer-afflicted individuals are reported to be 208 and 413 nM, respectively.[14] Thus, patient serum samples must be diluted 100- to 200-fold so that their CTAPIII + NAP2 concentrations fall within the dynamic range of the sensor binding isotherm. Figure 7B shows a linearized NAP2 binding isotherm for CLD **S3** under conditions simulating 200-fold sample dilution (0.5% fetal bovine serum), which would be suitable as an analytical calibration curve. The median serum CTAPIII+NAP2 levels for healthy and lung cancer afflicted individuals are readily distinguished considering the 95% confidence limits of the linear fit.

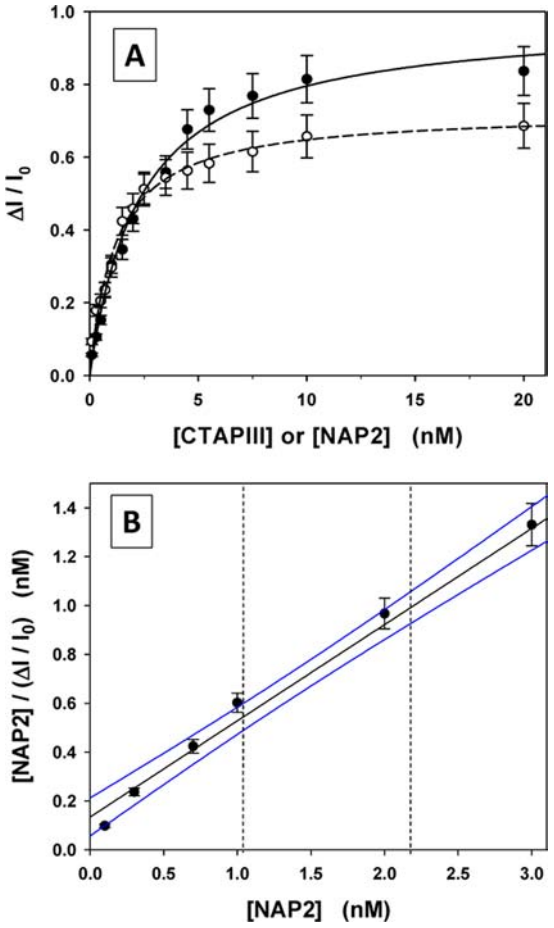

Figure 7. Electrochemical response of CLD **S3** as a function of CTAPIII or NAP2 concentration. (A) CLD **S3** response to NAP2 (●,—) and CTAPIII (○, ---) in binding buffer (serum-free). Fitted K_d values were 1.2 ± 0.1 nM for CTAP III and 2.4 ± 0.2 nM for NAP2 in binding buffer. (B) Linearized NAP2 binding isotherm for CLD **S3** in binding buffer supplemented with 0.5% fetal bovine serum. 200-fold dilution of clinical samples (to 0.5% serum) would be required for clinical analysis so that CTAP III + NAP2 concentrations fall within the dynamic range of the sensor. After 200-fold dilution, the median sample concentrations of CTAPIII + NAP2 for healthy and lung cancer afflicted individuals are 1.04 and 2.07 nM, respectively[14] (indicated by dashed vertical lines). Blue lines indicate the 95% confidence limits of the linear fit.

FRET Investigation of the Structural Basis for Sensor Function. The biochemical data, measured in solution, provide strong evidence that CLDs enhance three-way junction conductivity (through-DNA charge transport) in response to analyte binding (Figure 5B). However, in the gold electrode-bound context, although charge transport through duplex DNA from ferrocene to a gold electrode has been described,[19] the electrochemical signal observed in surface-bound CLDs could potentially arise from other charge transfer mechanisms. Two plausible alternative mechanisms could be: (1) switching between two distinctly different, and stable CLD conformations may significantly alter the distance between redox label and electrode and, thus, the rate of direct electron transfer between them;[5,6] or (2) changes in the flexibility of the CLD construct upon analyte binding could similarly alter the average distance between redox label and electrode.[20] The former charge transfer switching mechanism has served as the basis for a successful class of electrochemical sensors.[4−6] Therein, major structural changes, such as global folding of single stranded aptamers or secondary structure switching, draw a redox label closer to the electrode surface, increasing the rate of direct electron transfer between them.

We questioned whether in our system any major changes in CLD conformation or flexibility occur upon analyte binding (and concomitant switching of through-DNA charge transport, monitored biochemically). We felt that understanding this important point, using the CLD **S3**, may allow us to better account for charge transport switching in the electrode-bound form of CLD **S3**. We therefore undertook FRET experiments,[21] to probe for global conformational changes that might be triggered by analyte binding. In our design, the conductive stem termini of CLD **S3** serve as the attachment points to ferrocene and to the electrode surface, and a decrease in average distance between them (due to either structure switching or an increase in junction flexibility) would increase direct electron transfer rates. Inspired by the studies of 8−17 DNAzyme global folding by Lu and co-workers,[22] we attached Cy3 and Cy5 fluorophores to the respective conductive stem termini of CLD **S3** (Figure 8A) to gauge changes in the average distance between them upon analyte binding. We also used FRET to probe for global conformational changes within the aptamer domain that might underlie the switching mechanism. To do this, CLD **S3** was terminally labeled with Cy3 and internally labeled with Cy5 within the aptamer domain by conjugating C6-linked Cy5 to an amino-allyl-deoxyuridine that had been introduced in place of a nonconserved thymidine residue

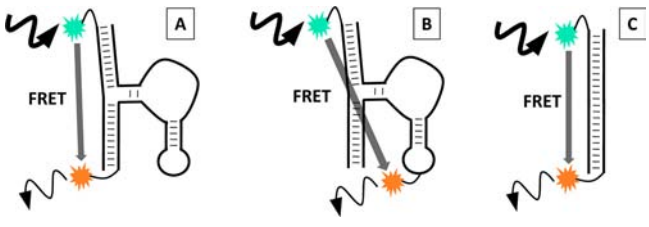

Figure 8. (A) CLD **S3** labeled with Cy3 and Cy5 at the termini of the reporter and detector stems, respectively. (B) CLD **S3** labeled with Cy3 at the terminus of the reporter stem, and internally labeled with Cy5 at a thymidine residue within aptamer domain in a loop of nonconserved sequence. (C) A 28-bp duplex with the same sequence as the sensor charge transport pathway terminally labeled with Cy3 and Cy5.

(Figure 8B). A Cy3/Cy5-labeled 28-bp duplex (Figure 8C), with the same sequence as the putative sensor charge transport pathway, was used as a control that represents the structural extreme for CLD **S3**, in which there is rigid, fully coaxial, stacking of the reporter and detector stems.

Before proceeding with FRET experiments, we first verified that the attachment of fluorophores to CLD **S3** did not adversely affect aptamer binding to CTAP III. Both of the fluorophore-labeled CLD **S3** constructs (Figure 8A,B) exhibited the expected electrophoretic mobility shift in the presence of CTAPIII in native gels (see Supporting Information). FRET emission spectra were recorded for each construct depicted in Figure 8 in buffer alone, and then following the sequential additions of each of 25 mM KCl, 1 mM $MgCl_2$, and 1 μM CTAPIII (see Supporting Information). FRET efficiencies, calculated from these spectra using eq 1 (Materials and Methods), are plotted in Figure 9. The FRET

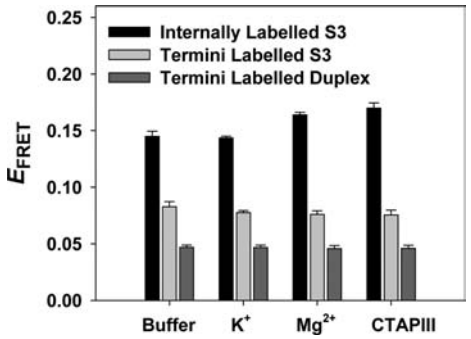

Figure 9. Plot of FRET efficiencies, calculated using eq 1, for the three Cy3/Cy5-labeled constructs shown in Figure 8. FRET efficiency was determined for each construct in buffer alone, and following the sequential addition of each of 25 mM KCl, 1 mM $MgCl_2$, and 1 μM CTAPIII. FRET spectra are shown in the Supporting Information.

efficiency for the terminally labeled 28 bp duplex control is constant under all conditions, and yields an estimated average interfluorophore distance of 99 Å (calculated using eq 2, Materials and Methods). This distance estimate provides validation for our FRET system as it is reasonable considering that the fluorophores are attached via flexible C6-linkers to a rigid 28 bp duplex 95 Å in length (assuming a typical base pair rise of 3.4 Å[23]).

The data in Figure 9 show that the FRET efficiency between Cy3 and Cy5 attached to the conductive stem termini of CLD **S3** decreases slightly upon addition of 25 mM K^+, but little further change is observed upon subsequent addition of 1 mM Mg^{2+} or 1 μM CTAPIII. These results indicate that no significant global change occurs in the relative equilibrium positions of the reporter and detector stems or in the junction flexibility of CLD **S3** upon analyte (CTAP III) binding. More subtle structural changes are likely to be in play that enable, in solution, the facilities charge transport through the two conductive stems (Figure 5). In the case of the internally labeled CLD **S3**, a small but noticeable change in FRET efficiency is detected upon addition of Mg^{2+} (Figure 9); this corresponds to a minimal structural change in which the interfluorophore distance changes by 2.1 Å. CTAP III binding (following Mg^{2+} addition) causes an even less distinct change in FRET efficiency for the internally labeled CLD **S3** (corresponding to a change in interfluorophore distance of 0.5 Å). Although FRET data provide only coarse-grained structural information, the results for both the internally and terminally labeled CLD **S3** constructs demonstrate that the structure of CLD **S3** does not change globally upon CTAP III binding.

With regard to the basis of conductivity switching in the electrochemical (chip-bound) version of this sensor, it is clear from the above FRET data that direct charge transfer in a distance-dependent manner, if it occurs, is not caused by gross analyte-induced changes in the conformation or flexibility of the sensor itself. The switching of through-DNA charge transport provides a much more straightforward mechanistic rationale that can account for each of the electrochemical signal switching, biochemical charge transport switching, and FRET results.

Notably, the sum of our above findings underscores the sensitivity of three-way junction conductivity switching to even *subtle* conformational changes induced by analyte binding to the aptamer domain. This, we believe, is a notable design advantage of this new class of DNA switch-based sensors. Such sensitivity will undoubtedly prove advantageous for a diversity of sensor design, as the aptamers that can be used for this class of sensors will not be limited to those that undergo global-scale structural changes upon analyte binding.

■ CONCLUSIONS

In summary, we have created a coupled ligand deoxyribosensor (CLD) that provides a simple, inexpensive means for quantifying a recently identified, and highly promising, early lung cancer biomarker. In so doing, we have established a general approach for the *de novo* creation of made-to-order sensors with electrochemical readout for newly discovered biomarkers. It is apparent that the design of CLD sensors based on biochemically observable through-DNA charge transport switching is "convertible" to successful electrochemical signal switching in electrode-bound CLDs. FRET data show no significant change in global structure on analyte binding, which argues against an electrochemical charge transfer switching mechanism involving direct charge transport from redox label to electrode. Therefore, we emphasize that CLDs represent a novel mechanistic design principle for aptamer sensors distinct from those designed to function based on large-scale structure switching events induced by analyte binding. As such, CLDs might be especially useful in cases where analyte binding produces only subtle aptamer conformational changes, rather than large-scale folding events that induce redox label relocation relative to the electrode surface.

We anticipate that the CLD approach will be easily adapted to enable the rapid creation of sensitive, yet portable CLDs for a wide range of analytes of environmental, medical, or other interest. We submit that CLDs provide a less cumbersome alternative to quantitative ELISA technologies, which require multiple sample manipulations as well as spectrophotometric instrumentation.[24] Moreover, in comparison to antibodies required for ELISA, DNA aptamers are much less costly, more easily obtained, more consistent from batch to batch, and more stable with a longer shelf life.[25] Therefore, aptamer-based CLDs should enable population-wide screening programs that might otherwise be prohibitively expensive with conventional diagnostic tests. A current goal is to incorporate the CTAPIII + NAP2 CLD described here into a practical device, that has the portability of a blood glucose meter and will provide rapid and accurate point-of-care diagnostic testing.

MATERIALS AND METHODS

Oligonucleotides for Biochemical CLD Experiments (Written 5′ to 3′).

CLD **S1**: TCACTATGGGAGCGAAGTTTTCTGGTATTA-TACCAGCCGTTACGCAATCTTAATCTCGTGAGCTAAA
CLD **S2**: TCACTATGGGAGCGAAAGGTTTTCTGGTAT-TATACCAGCCGTTACGCAATCCTTCTCGTGAGCTAAA
CLD **S3**: TCACTATGGGAGCGAGGTTTTCTGGTAT ***T*** ATACCAGCCGTTACGCAATCCTTCTCGTGAGCTAAA

Two Cy5-labeled CLD **S3** oligonucleotides were prepared for FRET experiments. Cy5 was attached via C6-linker at the 5′-terminus, or internally at the italicized thymidine residue in the sequence above. The internal label was introduced by substituting the nonconserved thymidine residue in the aptamer domain with amino-allyl-deoxyuridine, and reacting the primary amine so introduced with the C6-linked NHS-ester of Cy5.

CLD **S4**: TCACTATGGGAGCGAGGTTTTCTGGTATTA-TACCAGCCGTTACGCAATCCTAATCTCGTGAGCTAAA
CLD **S5**: TCACTATGGGAGCGTGGTTTTCTGGTATTA-TACCAGCCGTTACGCAATCCAAATCTCGTGAGCTAAA
CLD **S6**: TCACTATGGGAGCGCGGTTTTCTGGTATTA-TACCAGCCGTTACGCAATCCGAATCTCGTGAGCTAAA
AQ-oligonucleotide: $H_2N(CH_2)_6$O-TTTAGCTCACGA-GACGCTCCCATAGTGA
Biochemical charge transport control oligonucleotide: TCAC-TATGGGAGCGTCTCGTGAGCTAAA

A Cy3 labeled version of the AQ-oligonucleotide was also prepared for FRET experiments, where the C6-amino modification shown in the sequence above was replaced with C6-linked Cy3.

Oligonucleotides for Electrochemical CLD Experiments (Written 5′ to 3′).

CLD **S3**E: $HO(CH_2)_6$–S-S-$(CH_2)_6$O-TCTCCAGCGTC-GAGGTTTTCTGGTATTATACCAGCCGTTACG-CAATCCTTCTC GAGCTAAA
Fc-oligo: $H_2N(CH_2)_6$O-TTTAGCTCGAGACGACGCTGGA-GA
Fc-complement: $HO(CH_2)_6$-S-S-$(CH_2)_6$O-TCTCCAGCGTCGTCTCGAGCTAAA

***In Vitro* Selection of Aptamers.** Solid phase immobilization of CTAPIII and NAP2 was accomplished by reaction with NHS-activated 6% agarose beads (Pierce) in a coupling buffer containing 100 mM NaH_2PO_4 (pH 7.5)/150 mM NaCl for 45 min at room temperature (~100 nmol protein was reacted with 1 mL of bead suspension). The protein coupled beads were washed with 2 vol of coupling buffer, and the unreacted NHS-ester groups were blocked by reaction with 1 M ethanolamine-HCl (pH 8) at room temperature for 30 min. The blocked beads were washed with 2 vol of coupling buffer and stored at 4 °C in coupling buffer containing 0.05% sodium azide.

In the first round of selection, 10 nmol of PAGE purified, synthetic library DNA (5′-GTGTCCGAATGCGATTAGCA-$\mathbf{N}_{40}$-AGGCT-CAATCGGTCTGTATC) was combined with 20 pmol of 5′-^{32}P-labeled library DNA and heated to 100 °C for 2 min in 1 mL of TE buffer (10 mM Tris-HCl/0.1 mM EDTA) and cooled linearly in a PCR machine over the course of 15 min to 25 °C. 1.5 mL H_2O and 2.5 mL 2× selection buffer (SB) were then added and the sample was allowed to stand at room temperature for 10 min (final DNA concentration was 2 μM; 1× SB = 50 mM Tris-HCl/150 mM NaCl/5 mM KCl/10 mM $MgCl_2$). The DNA sample was then mixed with 0.5 mL of CTAPIII bead slurry that had been washed with the selection buffer, and this mixture was incubated at room temperature for 30 min with rolling. The supernatant was then decanted, and the resin was washed with 5 mL of 1× SB. DNA bound to the CTAPIII beads was then eluted with 0.5 mL 2 M NaOAc pH 5.2 followed by 1 mL TE buffer, both at room temperature. The eluates were combined, concentrated, and ethanol precipitated. The recovered DNA was PCR amplified using the following primers. Pfor, 5′-GTGTCCGAATGC-GATTAGC and Prev, 5′-GATACAGACC**r**GATTGAGCC (where rG is an embedded riboguanosine). The PCR program used was: 45 s at 95 °C, 30 s at 50 °C, 60 s at 72 °C. PCR products were pooled, ethanol precipitated, resuspended in 100 μL of 0.25 N NaOH, and heated for 10 min at 90 °C cleave the internal ribose linkage in the antisense strands. The samples were then neutralized with 11 μL of 3 M NaOAc (pH 5.2) and ethanol precipitated. The pellet was resuspended in standard denaturing PAGE loading solution (90% formamide/10 mM EDTA) and heated to 95 °C for 5 min. The sense strand was resolved from the shorter antisense strand by 7% denaturing PAGE, located by UV-shadowing, eluted into TE buffer, ethanol precipitated, and G-25 spin column desalted.

The amount of input DNA for selection was decreased to 500 pmol for rounds 2–6 and 100 pmol for rounds 7–15. The amount of CTAPIII beads was decreased to 250 μL for rounds 2–5, 100 μL for rounds 6 and 7, and 50 μL for rounds 8–15. The elution procedure was altered at round 3 because not all radioactivity that was bound to the CTAPIII beads could be eluted using the above elution procedure. For the remaining rounds, bead bound DNA was eluted with successive portions of 7 M urea/1× TBE heated to 100 °C for 2 min until no further radioactivity could be eluted. Negative selection was carried out in rounds 1, 2, 3, 14, and 15 by allowing the input DNA to bind to ethanolamine blocked agarose beads (without CTAPIII). The resulting supernatant was decanted and carried through the rest of the normal positive selection procedure for CTAPIII binding.

After the 15th round of selection, the remaining DNA pool was cloned into the pJet1.2 vector using the CloneJet kit (Fermentas). Twenty-five clones were picked and sequenced using the standard T7 promoter sequencing primer. Individual full length aptamer sequences were synthesized by PCR amplification of the clones using Pfor and Prev. The embedded ribose in the antisense strand was cleaved by NaOH treatment as in the selection procedure above. As the selection progressed, it was observed that the sense and antisense strands were not adequately denatured in standard formamide/EDTA PAGE loading solution (see Supporting Information). To ensure full denaturation, and PAGE separation of sense and antisense strands, the following PAGE loading procedure was adopted: after precipitation, the DNA pellet was resuspended in freshly prepared 90% formamide/50 mM NaOH/10 mM EDTA, heated at 100 °C for 5 min, and snap- cooled on ice before gel loading. Truncated aptamer sequences were prepared by solid phase synthesis and PAGE purified.

Electrophoretic Mobility Shift Assays. Trace amounts of 5′-^{32}P-labeled aptamer (final concentration <1 nM) were denatured in TE buffer for 2 min at 100 °C and allowed to cool at ambient temperature for 5 min. Aptamers were then made up in solution containing 0.2 mg/mL tRNA, 5% glycerol, 1× TB buffer, 25 mM KCl, 1 mM $MgCl_2$, and the desired CTAPIII concentration. After >10 min incubation at room temperature, samples were loaded, with running voltage applied, onto 8% native PAGE gels equilibrated at 4 °C. Native gels and the running buffer contained 1× TB buffer, 25 mM KCl, 1 mM $MgCl_2$ and were run at 5 W in a cold room (4 °C).

G- and T-Specific DNA Cleavage Reactions. Labeled aptamers were first denatured in TE buffer by heating to 100 °C for 2 min, followed by cooling at ambient temperature for 5 min. G-specific and T-specific cleavage reactions for protection analysis were performed in 40 μL reactions containing 200 mM Tris-HCl (pH 8) buffer and 1 mM EDTA, or 25 mM KCl/1 mM $MgCl_2$, or 25 mM KCl/1 mM $MgCl_2$/2 μM CTAPIII. All reactions contained 10 μg of tRNA and ca. 10 nM ^{32}P-labeled oligonucleotide. G-specific reactions were initiated by adding 4 μL of 10% dimethylsulfate (DMS) in ethanol, continued for 30 s at room temperature, and terminated by adding 2 μL of β-mercaptoethanol (neat). T-specific cleavage reactions were initiated by adding 4 μL of 2.4 mM $KMnO_4$, continued for 3 min at room temperature, and terminated by adding 2 μL of allyl alcohol (neat). All terminated reactions were immediately ethanol precipitated, washed with 70% ethanol, and dried. The samples were resuspended in 100 μL of 10% aqueous piperidine, heated at 90 °C for 30 min, and lyophilized extensively before standard 12% denaturing PAGE analysis.

Aptamer Domain Boundary Mapping Experiments. G-specific and T-specific cleavage reactions were performed as described above in 200 mM Tris-HCl/1 mM EDTA for both 5′- and 3′-^{32}P-labeled aptamer clone strands. Following piperidine treatment and extensive lyophilization, the samples were resuspended in 200 μL of 50 mM Tris-HCl (pH 8)/25 mM KCl/1 mM $MgCl_2$, heated to 100 °C for 2 min and cooled at ambient temperature for 5 min. These samples were mixed with 50 μL of CTAPIII conjugated agarose beads slurry and allowed to bind for 30 min at room temperature with gentle mixing by rolling the tubes. The beads were then pelleted by brief centrifugation, decanted, and washed with binding buffer until very little radioactivity could be detected in the wash (usually 3 or 4 washes). The bead bound aptamer fragments were then eluted by adding 100 μL of 7 M urea/TBE buffer and heating at 100 °C for 5 min. This procedure was repeated until most of the radioactivity had been released from the CTAPIII beads. The decanted binding buffer (unbound fragments) and denaturing elution samples (bound fragments) were then ethanol precipitated and compared by 12% denaturing PAGE.

Biochemical Assays of Coupled Ligand Deoxyribosensors. Anthraquinone was conjugated to the amino terminated AQ-oligo and the product was purified by HPLC (see Supporting Information). The CLD constructs were annealed by heating the 5′-anthraquinone-labeled oligo (AQ-oligo) and the 5′-^{32}P-labeled CLD oligo to 100 °C for 2 min in TE buffer and cooling at ambient temperature for 5 min. At this point, binding buffer was added, followed by the desired amount of CTAPIII. The final concentrations of both DNA strands were 125 nM. Samples were then transferred to a polystyrene 96-well ELISA plate which was equilibrated in contact with a water bath at 4 °C. Irradiation was carried out inside a cold room (4 °C) by placing the ELISA plate 4 cm below a UVP Black-Ray UVL56 lamp (365 nm) for 30 min. To ensure uniform irradiation, samples were loaded into only two rows of ELISA plate wells that were positioned equidistant from the UV lamp. Following irradiation, the samples were transferred to eppendorf tubes and ethanol precipitated. The dried DNA pellets were resuspended in 10% aqueous piperidine, heated to 90 °C for 30 min, and then lyophilized extensively. Samples were analyzed by 12% denaturing PAGE.

Preparation of Immobilized Coupled Ligand Deoxyribosensors on Gold Chips. Ferrocene was conjugated to the amino terminated Fc-oligo following an established protocol[26] and the product was purified by HPLC as described above for the AQ-oligo. The 5′-C6-thiol-terminated single-stranded DNA (**S3**E and Fc-complement oligos, 0.5−2.0 nmol) was generated by reduction of the precursor 5′-C6-disulfide DNA in 40 μL of 10 mM tris(2-carboxyethyl)phosphine hydrochloride (Sigma) in 100 mM Tris-HCl (pH 7.4) at room temperature for 12 h. Samples were desalted over MicroSpin G-50 columns (GE Health Care). The columns were equilibrated with deoxygenated water prior to use. DNA constructs to be immobilized on gold electrodes were prepared by combining freshly prepared HS-DNA (5.0 μM **S3**E oligo or 5.0 μM Fc-complement oligo) with the 5.5 μM Fc oligo in deoxygenated CTAPIII/NAP2 binding buffer (50 mM Tris-HCl, 25 mM KCl, 1 mM $MgCl_2$, pH 8.0). Samples were annealed by heating to 80 °C for 2 min, followed by slow cooling to room temperature.

Gold substrate slides (100 nm Au/5 nm Cr/glass) were purchased from Evaporated Metal Films Inc. (Ithaca, NY). Prior to modification, they were cleaned with freshly prepared piranha solution (3:1 v/v mixture of concentrated H_2SO_4 and 30% H_2O_2) at 90 °C for 5 min and then rinsed thoroughly with water [***Caution!*** *piranha solution reacts violently with organic material*]. The annealed CLD constructs were immobilized by spreading a 50-μL droplet over a ∼1 cm^2 area of the cleaned gold substrate for 12 h at 100% humidity. The gold chips were then rinsed with 0.5 mL binding buffer three times, immersed in 20 μM 6-mercaptohexanol (in binding buffer) for 4 h to passivate the gold surface, and rinsed again as above. Chips were stored at 100% humidity and electrochemical characterization was carried out within 24 h.

Electrochemical Measurements of CTAP III/NAP2 Coupled Ligand Deoxyribosensor. Electrochemical measurements were carried out in a home-built, 1 mL three-electrode cell. The gold chip served as the working electrode and was sealed against an O-ring at the bottom of the cell so that an area of 0.126 cm^2 of gold surface was exposed to the test solution. A platinum wire counter electrode and Ag|AgCl|1 M KCl reference electrode were immersed in the test solution. Cyclic voltammetry (CV) and square wave voltammetry (SQW) measurements were performed at ambient temperature (21−23 °C) using μ-Autolab II potentiostat/galvanostat (Eco Chemie B.V., Utrecht, Netherlands). The parameters for square wave measurements were as follows: preconditioning for 5 s at +0.45 V; initial potential = +0.45 V; final potential = −0.1 V; step potential = 0.002 V; step amplitude = 0.2 V; frequency = 15 Hz. Measurements were made in binding buffer, or various dilutions of fetal bovine serum (Sigma) in binding buffer, before and after 10 min incubation with various concentrations of CTAPIII, NAP2 or other control proteins.

FRET Experiments. Fluorophore-labeled oligonucleotides were annealed as described above in TE buffer with oligonucleotide concentrations of 10 μM each. Samples were made up to 10% glycerol and loaded onto 8% native PAGE gels (40 mM Tris-borate buffer, pH 8.3) run at 4 °C. CLD **S3** and duplex complexes were well resolved from single stranded oligonucleotides (see Supporting Information), and the appropriate bands were excised from the gel and eluted by crush and soak (overnight at 4 °C) into ∼10 gel volumes of 40 mM Tris-borate. Gel purified complexes were maintained at 4 °C during storage and all manipulations. Eluted sample concentrations were determined by UV−vis absorption measurement at 260 nm. All samples for FRET experiments initially contained: 80 nM purified complex (CLD **S3** or duplex), 50 mM Tris-HCl (pH 8.0), 8 mM Tris-borate, and 1 mg/mL glycogen. After recording emission spectra under the initial conditions, 25 mM KCl, 1 mM $MgCl_2$, and 1 μM CTAPIII were added sequentially, with emission spectra recorded after each of these additions.

Steady state fluorescence emission spectra were recorded at 4 °C on a Fluoromax 3 fluorimeter (Horiba/Jobin Yvon). Polarization artifacts were minimized by crossing the polarizers at the "magic angle" (excitation polarizer: 0°, emission polarizer: 54.7°).[21] Spectra were corrected for lamp intensity, background spectra were subtracted, and an instrument-specific correction was applied ("MCORRECT"). FRET efficiencies were calculated using the $(\text{ratio})_A$ method, which has been reviewed in detail by Clegg.[21] The work of Lu and co-workers, who studied 8−17 DNAzyme folding using the Cy3/Cy5 donor/acceptor pair,[22] was particularly relevant to the present study. Briefly, the quantity $(\text{ratio})_A$ is the ratio of acceptor emission intensity due to FRET (upon donor excitation at λ_{ex}^{D} = 513 nm) to acceptor emission intensity upon direct excitation of the acceptor at λ_{ex}^{D} = 648 nm. Because the donor and acceptor emission spectra overlap, the former must be subtracted from the FRET spectrum to obtain the acceptor emission intensity due to FRET (see Supporting Information). The value of $(\text{ratio})_A$ is thus calculated according to:[21,22]

$$(\text{ratio})_A = \frac{F^{AD}(\lambda_{em}, \lambda_{ex}^{D}) - \alpha F^{D}(\lambda_{em}, \lambda_{ex}^{D})}{F^{AD}(\lambda_{em}, \lambda_{ex}^{A})} = \frac{\varepsilon^{A}(\lambda_{ex}^{D})}{\varepsilon^{A}(\lambda_{ex}^{A})} + d^{+}E_{FRET}\frac{\varepsilon^{D}(\lambda_{ex}^{D})}{\varepsilon^{A}(\lambda_{ex}^{A})} \quad (1)$$

Where $F^{AD}(\lambda_{em},\lambda_{ex}^{D})$ is the emission intensity of the dual labeled complex at the donor excitation wavelength, $F^{D}(\lambda_{em},\lambda_{ex}^{D})$ is the emission intensity of the donor only labeled complex, $F^{AD}(\lambda_{em},\lambda_{ex}^{A})$, and α is a weighting factor obtained by fitting the donor only spectrum to the FRET spectrum over the wavelength range where the acceptor does not emit (525−600 nm). The FRET efficiency (E_{FRET}) can then be calculated once the necessary extinction coefficient ratios have been determined from absorption spectra. For HPLC purified samples, as used in this study, the fraction of DNAs labeled with the Cy3 donor (d^+) is taken as 100%.

Average distances (R) between FRET donor and acceptor were estimated from E_{FRET} values based on the relationship:[21,22]

$$F_{FRET} = \frac{R_0^6}{R_0^6 + R^6} \quad (2)$$

where R_0 is the donor−acceptor separation at which the FRET efficiency is half maximal. R_0 is related to the value of an orientation factor, κ, which describes the directional orientation of the fluorophore transition dipole moments.[21,27] Studies by Lilley and co-workers suggest that C3-linked cyanine fluorophores can stack upon the blunt ends of DNA helices to some extent (here we use C6-linked Cy3 and Cy5) so as to limit the rotational freedom of the fluorophores,[27] which affects the value of κ and R_0.[21] Nevertheless, the 5′-C6-linked Cy3/Cy5 FRET pair has been used previously with great success to study folding transitions in nucleic acids.[19] For our purposes of estimating the change in distance between the Cy3- and Cy5-labeled helical termini, we make the simplifying assumption that the fluorophores can freely rotate, in which case $\kappa = 2/3$. Using eq 2 and a value of 60 Å for R_0 (from ref 21) leads to a reasonable average distance estimate in the case of the rigid duplex control (see Results and Discussion).

■ ASSOCIATED CONTENT

Supporting Information

Detailed experimental procedures and additional data for protein expression, *in vitro* selection, aptamer characterization, and biochemical and electrochemical charge transport studies. This material is available free of charge via the Internet at http://pubs.acs.org.

■ AUTHOR INFORMATION

Corresponding Author

sen@sfu.ca; hogan_yu@sfu.ca

Notes

The authors declare no competing financial interest.

■ ACKNOWLEDGMENTS

This research was funded by the Natural Sciences and Engineering Research Council of Canada (NSERC), the Canadian Institutes of Health Research (CIHR), and the Canadian Institute for Advanced Research (CIFAR). D.S. is a fellow of CIFAR.

■ REFERENCES

(1) (a) O'Sullivan, C. K. *Anal. Bioanal. Chem.* **2002**, *372*, 44−48. (b) Nutiu, R.; Li, Y. *Methods* **2005**, *37*, 16−25. (c) Song, S.; Wang, L.; Li, J.; Zhao, J.; Fan, C. *Trends Anal. Sci.* **2008**, *27*, 108−117. (d) Liu, J.; Lu., Y. *Angew. Chem.* **2006**, *45*, 90−94. (e) Chen, H. W., Kim, Y., Meng, L., Mallikaratchy, P., Martin, J., Tang, Z., Shangguan, D., O'Donoghue, M., Tan, W. *Functional Nucleic Acids for Analytical Applications*; Li, Y., Lu, Y., Eds.; Springer: New York, 2009; pp 111−130; (f) Rupcich, N., Nutiu, R., Shen, Y., Li, Y., Brennan, J. D. *Functional Nucleic Acids for Analytical Applications*; Li, Y., Lu, Y., Eds.; Springer: New York, 2009; pp 309−342; (g) Liu, J.; Cao, Z.; Lu, Y. *Chem. Rev.* **2009**, *109*, 1948−1998.

(2) (a) Medley, C. D.; Smith, J. E.; Tang, Z.; Wu, Y.; Bamrungsap, S.; Tan, W. *Anal. Chem.* **2008**, *80*, 1067−1072. (b) Xu, Y.; Phillips, J. A.; Yan, J.; Li, Q.; Fan, Z. H.; Tan, W. *Anal. Chem.* **2009**, *81*, 7436−7442. (c) Medley, C. D.; Bamrungsap, S.; Tan, W.; Smith, J. E. *Anal. Chem.* **2011**, *830*, 727−734.

(3) (a) Nutiu, R.; Li, Y. *J. Am. Chem. Soc.* **2003**, *125*, 4771−4778. (b) Nutiu, R.; Li, Y. *Chem.—Eur. J.* **2004**, *10*, 1868−1876. (c) Liu, J., Lu, Y. *Functional Nucleic Acids for Analytical Applications*; Li, Y., Lu, Y., Eds.; Springer: New York, 2009; pp 155−178; (d) Cho, E. J.; Lee, J.-W.; Ellington, A. D. *Ann. Rev. Anal. Chem.* **2009**, *2*, 241−264.

(4) For reviews see: (a) Willner, I.; Zayats, M. *Angew. Chem.* **2007**, *46*, 6408−6418. (b) Cheng, A. K. H.; Sen, D.; Yu, H.-Z. *Bioelectrochemistry* **2009**, *77*, 1−12. (c) Li, D.; Song, S.; Fan, C. *Acc. Chem. Res.* **2010**, *43*, 631−641. (d) Lubin, A. A.; Plaxco, K. W. *Acc. Chem. Res.* **2010**, *43*, 496−505.

(5) (a) Xiao, Y.; Lubin, A. A.; Heeger, A. J.; Plaxco, K. W. *Angew. Chem.* **2005**, *44*, 5456−5459. (b) Radi, A.-E.; Sánchez, J. L. A.; Baldrich, E.; O'Sullivan, C. K. *J. Am. Chem. Soc.* **2006**, *128*, 117−124. (c) Ferapontova, E. E.; Olsen, E. M.; Gothelf, K. V. *J. Am. Chem. Soc.* **2008**, *130*, 4256−4258. (d) Uzawa, T.; Cheng, R. R.; White, R. J.; Makarov, D. E.; Plaxco, K. W. *J. Am. Chem. Soc.* **2010**, *132*, 16120−16126.

(6) (a) Xiao, Y.; Piorek, B. D.; Plaxco, K. W.; Heeger, A. J. *J. Am. Chem. Soc.* **2005**, *127*, 17990−17991. (b) Zuo, X.; Song, S.; Zhang, J.; Pan, D.; Wang, L.; Fan, C. *J. Am. Chem. Soc.* **2007**, *129*, 1042−1043. (c) Lu, Y.; Li, X.; Zhang, L.; Yu, P.; Su, L.; Mao, L. *Anal. Chem.* **2008**, *80*, 1883−1890.

(7) Polski, R.; Gill, R.; Kaganovsky, L.; Willner, I. *Anal. Chem.* **2006**, *78*, 2268−2271.

(8) Fahlman, R. P.; Sen, D. *J. Am. Chem. Soc.* **2002**, *124*, 4610−4616.

(9) Sankar, C. G.; Sen, D. *J. Mol. Biol.* **2004**, *340*, 459−467.

(10) Huang, Y. C.; Ge, B.; Sen, D.; Yu, H.-Z. *J. Am. Chem. Soc.* **2008**, *130*, 8023−8029.

(11) (a) Kelley, S. O.; Jackson, N. M.; Hill, M. G.; Barton, J. K. *Angew. Chem., Int. Ed.* **1999**, *38*, 941−945. (b) Long, Y.-T.; Li, C.-Z.; Sutherland, T.-C.; Chahma, M.; Lee, J. S.; Kraatz, H.-B. *J. Am. Chem. Soc.* **2003**, *125*, 8724−8725. (c) Wong, E. L. S.; Gooding, J. J. *J. Am. Chem. Soc.* **2007**, *129*, 8950−8951.

(12) (a) Jemal, A.; Siegel, R.; Ward, E.; Murray, T.; Xu, J.; Thun, M. J. *CA Cancer J. Clin.* **2007**, *57*, 43−66. (b) Parkin, D. M.; Bray, F.; Ferlay, J.; Pisani, P. *CA Cancer J. Clin.* **2005**, *57*, 74−108.

(13) Yee, J.; Sadar, M. D.; Sin, D. D.; Kuzyk, M.; Xing, L.; Kondra, J.; McWilliams, A.; Man, S.F. P.; Lam, S. *J. Clin. Oncol.* **2009**, *27*, 2787−2792.

(14) Duncan, M. W. *J. Clin. Oncol.* **2009**, *27*, 2749−2750.

(15) Lee, G.; Gardner, B. K.; Elashoff, D. A.; Purcell, C. M.; Sandha, H. S.; Mao, J. T.; Krysan, K.; Lee, J. M.; Dubinett, S. M. *Am. J. Transl. Res.* **2011**, *3*, 226−233.

(16) (a) Proudfoot, A. E. I.; Peitsch, M. C.; Power, C. A.; Allet, B.; Mermod, J.-J.; Bacon, K.; Wells, T. N. *J. Protein Chem.* **1997**, *16*, 37−49. (b) Malkowski, M. G.; Wu, J. Y.; Lazar, J. B.; Johnson, P. H.; Edwards, B. F. P. *J. Biol. Chem.* **1995**, *270*, 7077−7087.

(17) (a) Ellington, A. D.; Szostak, J. W. *Nature* **1990**, *346*, 818−822. (b) Tuerk, C.; Gold, L. *Science* **1990**, *249*, 505−510.

(18) (a) Assenberg, R.; Weston, A.; Cardy, D. L. N.; Fox, K. R. *Nucleic Acids Res.* **2002**, *30*, 5142−5150. (b) van Buuren, B. N.; Overmars, F. J.; Ippel, J. H.; Altona, C.; Wijmenga, S. S. *J. Mol. Biol.* **2000**, *304*, 371−383. (c) Leontis, N. B.; Hills, M. T.; Piotto, M.; Ouporov, I. V.; Malhotra, A.; Gorenstein, D. G. *Biophys. J.* **1995**, *68*, 251−265. (d) Welch, J. B.; Walter, F.; Lilley, D. M. *J. Mol. Biol.* **1995**, *251*, 507−519. (e) Welch, J. B.; Walter, F.; Lilley, D. M. *Nucleic Acids Res.* **1993**, *21*, 4548−4555.

(19) Long, Y.-T.; Li, C.-Z.; Sutherland, T.-C.; Chahma, M.; Lee, J. S.; Kraatz, H.-B. *J. Am. Chem. Soc.* **2003**, *125*, 8724−8725.

(20) (a) Anne, A.; Demaille, C. *J. Am. Chem. Soc.* **2006**, *128*, 542−557. (b) Anne, A.; Bouchardon, A.; Moiroux, J. *J. Am. Chem. Soc.* **2003**, *125*, 1112−1113.

(21) Clegg, R. M. *Methods Enzymol.* **1992**, *211*, 353−388.

(22) (a) Kim, H.-K.; Liu, J.; Li, J.; Nagraj, N.; Li, M.; Pavot, C.M.-B.; Lu, Y. *J. Am. Chem. Soc.* **2007**, *129*, 6896−6902. (b) Mazumdar, D.; Nagraj, N.; Kim, H.-K.; Meng, X.; Brown, A. K.; Sun, Q.; Li, W.; Lu, Y. *J. Am. Chem. Soc.* **2009**, *131*, 5506−5515.

(23) Voet, D., Voet, J. G. *Biochemistry*; John Wiley & Sons: New York, 1995.

(24) DuoSet CXCL7/NAP2 ELISA Kit, Cat. No. DY393, R & D Systems, Minneapolis, MN.

(25) (a) Keefe, A. D.; Pai, S.; Ellington, A. D. *Nat. Rev. Drug Discovery* **2010**, *9*, 537−550. (b) Cho, E. J.; Lee, J. W.; Ellington, A. D. *Annu. Rev. Anal. Chem.* **2009**, *2*, 241−64. (c) Mok, W.; Li, Y. *Sensors* **2008**, *8*, 7050−7084.

(26) Ihara, T.; Maruo, Y.; Takenaka, S.; Takagi, M. *Nucleic Acids Res.* **1996**, *24*, 4273−4280.

(27) Iqbal, A.; Arslan, S.; Okumus, B.; Wilson, T. J.; Giraud, G.; Norman, D. G.; Ha, T.; Lilley, D. M. J. *Proc. Natl. Acad. Sci. U.S.A.* **2008**, *105*, 11176−11181.